Kuwait J.Sci., Vol.50, No.(3B),July.2023,pp(1-13)

Impedance analysis of single walled carbon nanotube/vinylester polymer composites

*Aykut Ilgaz

Dept. of Physics, Balıkesir University, Balıkesir, Turkey

** Corresponding author: aykut17ilgaz@gmail.com*

Abstract

This study presents impedance characteristics of single walled carbon nanotube/vinylester (SWCNT/VE) glass fiber reinforced polymer (GFRP) composites. The impedance measurements were carried out as a function of the frequency over range of 10^{-2} and 10^{7} Hz at various temperatures between 300 K and 420 K. Bode and Nyquist plots of real and imaginary parts of complex impedance (Z*) were obtained and Cole–Cole approach was used to interpret the impedance characteristics. The results indicated that the bulk resistance of the material decreases significantly as the temperature increases. The frequency-dependent AC conductivities were calculated using the complex impedance data and dimensions of specimen. It has been observed that the alternating current values are compatible with the Jonscher's power law. The behavior of dielectric constant and loss factor at the various temperatures were analyzed as a function of applied frequency. While the sample exhibited high dielectric permittivity in the low frequency region with the Maxwell-Wagner-Sillars (MWS) effect, it was observed that the permittivity decreased as a result of the dipoles' inability to rotate themselves in the field direction at high frequencies. No dielectric relaxation peak was observed in the loss spectra in our limits. From the results, it can be said that the contribution to the dielectric relaxation is due to the interface polarization and DC conductivity. Electric modulus formalism was also used to describe the conductivity and dielectric relaxation processes of SWCNT/VE binary composite. It was found that the obtained peak maximums shifted to higher frequencies as the temperature increased. It is concluded that the frequency regime below the peak maximum defines the range of mobile charge carriers, and in the regime above the maximum, the charge carriers are limited to short distance potential wells.

Keywords: Dielectric properties; electric modulus; impedance; single walled carbon nanotubes; vinylester resin.

1. Introduction

Since their discovery in the early 90s, carbon nanotubes have been used as high-potential reinforcement elements in many applications such as field-effect transistors (Liang *et al.*, 2015), energy storage (Zhu *et al.*, 2014), sensors (Daliri *et al.*, 2018) and composites (Kuilla *et al.*, 2010) over the past 30 years. The number of studies on the use of carbon nanotubes (CNTs) as a

reinforcement additive in traditional glass fiber reinforced polymer (GFRP) composites has increased considerably in the last two decades (Mahapatra *et al.*, 1991; Bouzerara *et al.*, 2011; Puertolas *et al.*, 2017; Das & Dobbidi, 2021). Many researchers reported impedance characteristics, conductivity mechanisms including percolating system, and relaxation phenomena of carbon nanotube reinforced composites (Antonucci *et al.*, 2007; Dang *et al.*, 2011; An *et al.*, 2013; Almuhammadi *et al.*, 2017; Anju & Narayanankutty, 2019; Ganesh *et al.*, 2020).

It is reported dielectric behavior of carbon nanotubes particles-filled polyester polymer composites at different temperatures using the Cole-Cole approach (Samir *et al.*, 2017). It has been proven that AC conductivity increases with increasing nanotube ratio and temperature. Aviles *et al.* studied the conductivity mechanism in the carbon nanotubes reinforced vinylester-based polymer composites. High conductivity is obtained even at low nanotube densities exceeding the percolation threshold (Aviles *et al.*, 2018).

The dielectric and impedance characteristics of multi-walled carbon nanotube (MWCNTs) and graphene oxide-carbon nanotube (GCNTs) reinforced acrylonitrile–butadiene–styrene (ABS) composites were studied comparatively (Jyoti *et al.*, 2018). It has been demonstrated that the materials can be used in electromagnetic interference (EMI) shielding and antistatic materials due to their improved conductivity. The dielectric properties of the MWCNT-modified polyester resin-based composite were investigated and MWCNT-filled polyester-based composites with high dielectric loss were proven to be quality materials for electromagnetic shielding applications (Seng *et al.*,2018).The capacitive behavior was explained by the charge accumulation on the surfaces of the carbon nanotubes, and the resistive behavior with the tunneling mechanism of the electrons in multi-walled carbon nanotubes-polydimethylsiloxane (PDMS) elastomer composites (Helseth ,2018). It was characterized by the electrical properties and relaxation processes of carbon nanotubes filled epoxy polymer composites using electrical modulus formalism. The dipolar and Maxwell-Wagner-Sillars (MWS) relaxations were investigated depending on filler concentration and temperature using the Havriliak-Negami model (Boukheir *et al.*, 2018).

The present study aims to determine accurately complex impedance, complex dielectric function, and AC conductivity properties for extracting new information about the charge transport mechanism and relaxation process of SWCNT/VE binary composites using impedance spectroscopy in the frequency range 10^{-2} Hz to 10^{7} Hz. Bode and Nyquist plots were used to explain real and imaginary impedance components with the Cole-Cole approach. The electrical behavior of the composite was studied depending on temperature and frequency. It is found that the material has exceeded the percolation threshold and a conduction network was formed throughout the material even at low temperatures. The complex dielectric function analysis was also carried out depending on the frequency at low and high temperatures. To bring a different perspective to the relaxation phenomenon, electrical modulus formalism has been applied to the system in addition to dielectric function analysis.

2. Experimental procedure

2.1 Material

The sample used in this study was produced by the hot press method and contains vinylester resin (acid value max. 9 mg KOH/gr, monomer content 42 %, density 1.04 g/cm^3), single walled carbon nanotube (purity > 90 wt. %, diameter 10–25 nm, length 20 μm, density 1.87 g/cm^3, flash point >150 °C), glass fiber FWR6 (filament diameter 17 μm). In addition to these three important components, the composite product includes peroxide, styrene, zinc sulfide, calcium carbonate, thickening admixture and additives. The percentages by weight of the components that form the material are shown in Figure 1.

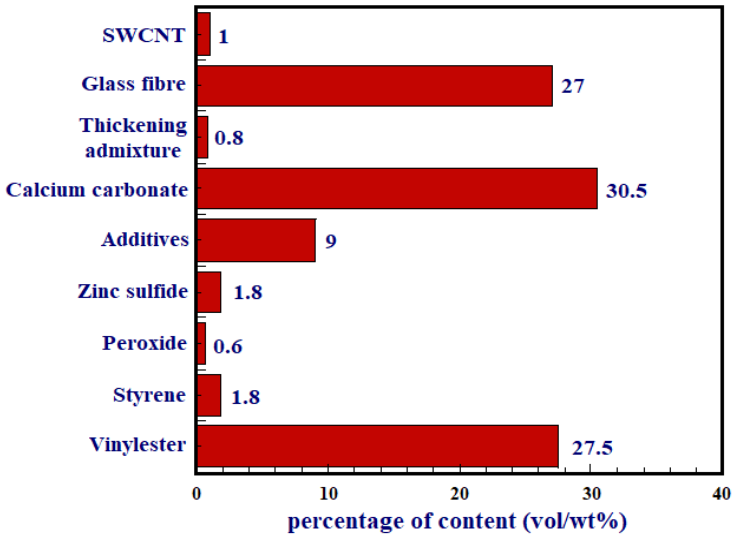

Fig. 1. Components of SWCNT/VE composite

In the production phase, components and vinylester resin were mixed mechanically continuously with the mixer to prevent agglomeration of the components and carbon nanotubes and to increase their integration with each other. When the mixture became viscous pulp, it was transferred onto polyethylene foils. At this point, glass fiber was added to the pulp laid on the carrier band. Another layer of pulp was placed on top of the pulp containing glass fiber chopped. The sandwich structure was passed between the rotating rollers to prevent the gaps between the pulps. The carrier films on the pulps were removed and the material was weighed and placed in the mold brought to the appropriate temperature in the hydraulic press. The pulps softened under high temperature and pressure and flowed into the mold cavity and thus took the desired shape. The molding temperature was 120-160℃ and the mold pressure was 80-140 Barr. At the end of the molding period of about 2 minutes, the materials were pressed on the test plates.

2.2 Morphology

SEM analyzes were performed to examine the distribution of components and SWCNTs in the glass fiber reinforced thermosetting vinylester resin-based composite structure and the relevant photographs are presented in Figure 2. Although there was agglomeration in certain regions, the random distribution of SWCNTs into the matrix resulted in a nearly homogeneous structure and it can be said that the single carbon nanotube exhibited well dispersion. As can be understood from the AC conductivity measurements, 1 wt. % of SWCNTs dispersed in the matrix formed a fully 3-dimensional conductivity network throughout the material at room temperature.

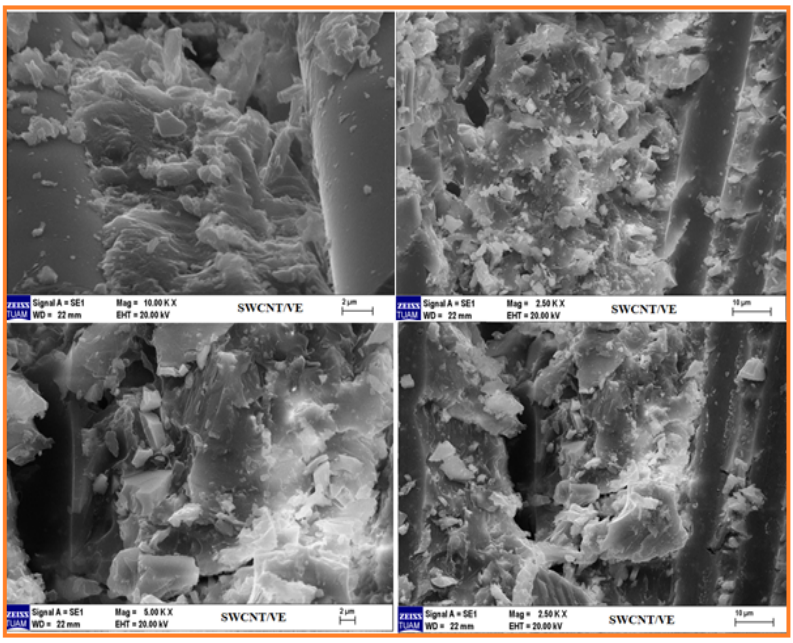

Fig. 2. SEM images of SWCNT/VE composites.

3. Results and discussion

3.1 Complex Impedance

The impedance spectroscopy of SWCNT/VE/GFRP was performed by MFIA Impedance Analyzer in the frequency range 10^{-2} Hz–10^{7} Hz with amplitude of 1 V voltage. Specimens with 15 mm length, 8 mm width and 7 mm thickness were deposited between parallel round plate electrodes. A carbon layer was coated on surface of the specimen to make the electrical contact better. The complex impedance (Z^{*}) was found as a function of frequency from impedance measurements at different temperatures. The real part (Z') of complex impedance denotes the resistance of the material while imaginary part (Z'') describes loss factor (Jyoti *et al.*, 2018).

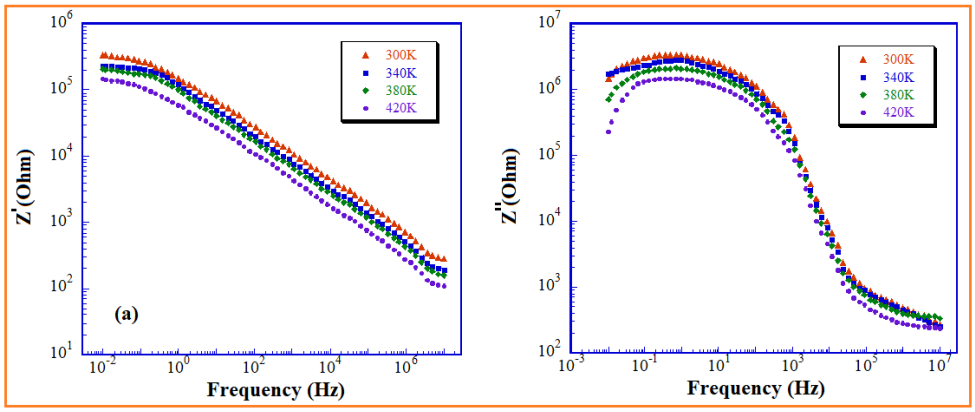

Fig. 3. Bode plots of real and imaginary impedance at different temperatures.

Figure 3 shows Bode plots of Z' and Z'' of SWCNT/VE polymer composite at various temperatures between 300 K and 420 K. As can be seen from the Figure. 3 (a), although the Z' value gives an almost constant appearance at very small frequencies, it decreases monotonically with the increase in frequency at all temperature measurements because of the weakening interface polarization. Figure.3 (b) shows the Z'' characteristics for SWCNT/VE binary composite as a function of temperature and frequency. Maximum was observed at low-frequency regions for all measurements. Maximums in the Z'' graph highlight the presence of dipolar relaxation in that frequency region. It can be also seen that both real and imaginary impedance components are frequency-dependent rather than the temperature.

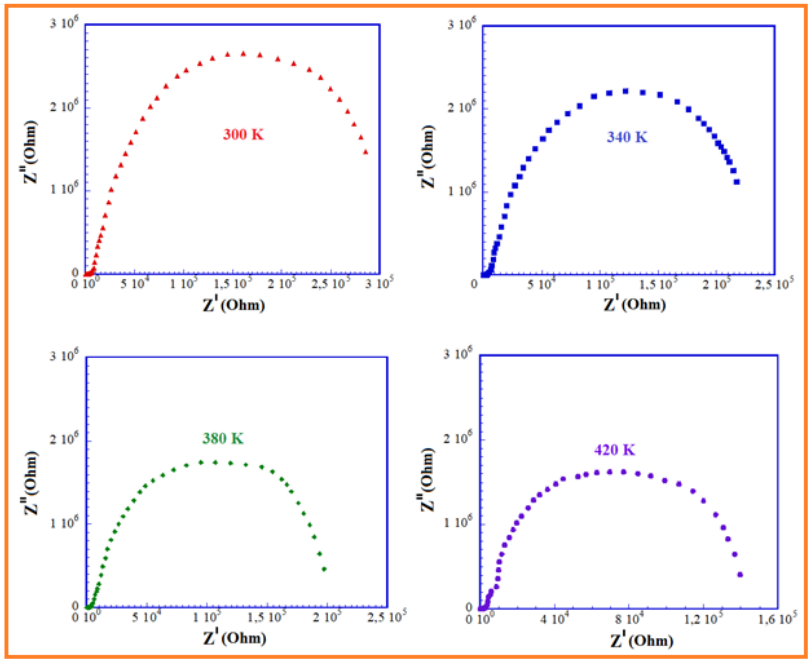

Fig. 4. Nyquist plots of SWCNT/VE composites at various temperatures.

Figure 4 shows Nyquist plots of the complex impedance of the SWCNT filled GFRP composites at various temperatures. A typical shape of Cole-Cole graphs is a semicircle that is almost reached at high-temperature values. When the maximums of the graphs are examined comparatively, the measurement with the smallest diameter magnitude of the possible semicircles is the measurement at 420 K. The electrical conductivity in composite films depends on the radius of arc in complex plane graphs. A large arc radius represents low conductivity and a low arc radius depicts higher conductivity values (Ho *et al.*, 2008). It can be said from plots that the resistance of the composite decreases as temperature increases, conductivity increases, and a less viscous media occurs at 420 K.

3.2 Alternating conductivity (AC)

Disordered conductive materials such as polymer composites show a similar response to the applied electric field as the dielectric response. Conductivity process is characterized by the real part σ′ (ω) of the complex electrical conductivity. This component, which is mostly frequency dependent, is known alternating current (AC) conductivity. The AC conductivity consists of two parts and is expressed as (Jonscher, 1977; Almond *et al.*, 1982; Tsonos, 2019):

$$\sigma'(\omega) = \sigma_0 + k.\omega^s \quad (1)$$

where σ_o is the frequency-independent DC conductivity, k is the constant, ω is the angular frequency and s is the exponent with value ranging of 0-1.

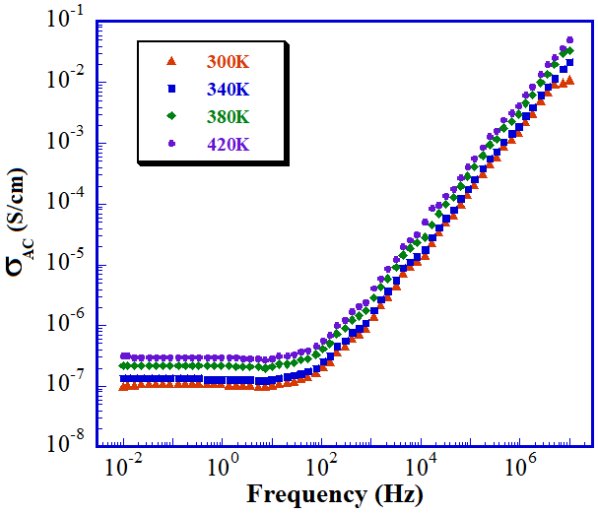

Fig. 5. AC conductivities of SWCNT/VE/GFRP at various temperatures.

It was observed from Figure. 5 that AC conductivities at all temperatures exhibited frequency-independent behaviors in the low-frequency regime. This means that the percolation threshold was exceeded in the SWCNT/VE composite with 1 SWCNT wt. % and the conduction network was ensured directly between the nanotube particles within the polymer matrix at a low-frequency regime. In this region, the conductivity value obtained at high temperatures is

approximately 3 times the value at low temperatures. The AC conductivities showed a linear dependence with frequency after 100 Hz obeying the Jonscher's power law as given in Eq. (1). AC conductivity values are more frequency-dependent than the temperature at high frequencies with similar impedance behavior.

3.3 Dielectric Characteristics

Dielectric analysis determines the real and imaginary components of the complex dielectric function depending on the frequency with the response of a dielectric material to alternating current. The complex dielectric function is expressed as (Boukheir *et al*., 2018; Savi *et al*., 2019):

$$\varepsilon^*(\omega) = \varepsilon'(\omega) - j\varepsilon''(\omega) \quad (2)$$

where ε'(ω) and ε"(ω) correspond to the real and imaginary parts of the complex dielectric function, respectively. The real part of the dielectric function is energy storage component and is known as dielectric constant. Dielectric constant is given by (Jyoti *et al.*, 2018):

$$\varepsilon'(\omega) = {Z''}/{2\pi f C_0 Z^2} \quad (3)$$

where f is frequency and C_0 is the geometrical capacitance of sample. Capacitance is defined by the equation (Philipose *et al.*, 2021)

$$C_0 = {\varepsilon_0 A}/{d} \quad (4)$$

where ε_o is the dielectric constant of vacuum, A is area and d is thickness. The imaginary component represents the energy loss due to conduction losses, vibration losses and polarization and is called loss factor (Lvovich, 2012). Contributions to the loss factor originate from interface polarization, DC conductivity and dipole orientations. Loss factor is described as (Jyoti *et al.*, 2018)

$$\varepsilon''(\omega) = {Z'}/{2\pi f C_0 Z^2} \quad (5)$$

Figure. 6 (a) shows the variation of ε' with applied frequency at different temperatures. It is seen that ε' values depend on frequency at all temperatures. The high values of ε' is shown from the graph at low frequencies due to the charge accumulation at the interface between the insulating region and conductive additives. Since the accumulated charges partly block the external electric field, the dielectric constant increases at these frequency values. The Maxwell-Wagner-Sillars process is an effective mechanism in this frequency regime (Dang *et al.*, 2007; Belhimria *et al.*, 2021). When the frequency of the field is gradually increased, the dipoles can't find enough time to align themselves with the field and the dielectric permittivity is reduced (Mergen *et al.*, 2020).

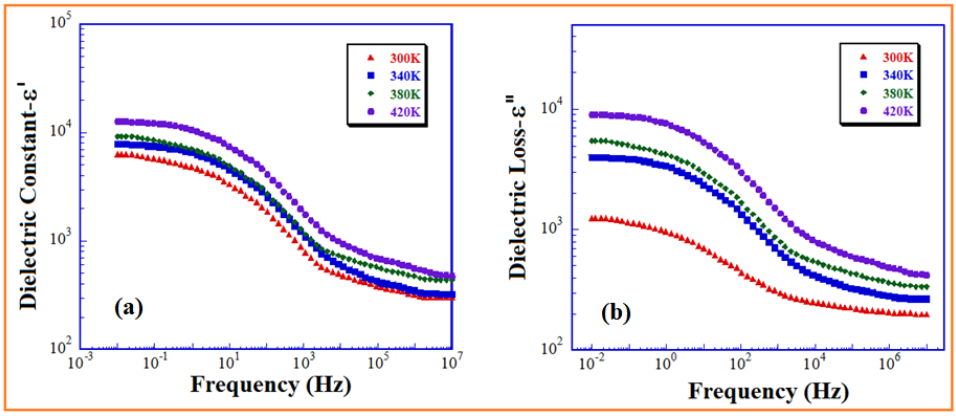

Fig. 6. (a) dielectric constant and (b) dielectric loss depending on frequency.

Figure. 6 (b) shows the plot of the loss factor as a function of frequency at different temperatures. It is seen that the increase in temperature affects the dielectric loss. As the temperature increases, thermally excited dipoles increase the peak value of the losses by following the change of the applied electric fields. Therefore, the loss factor values at 420 K are higher than the other measurements. As shown from the graph, no loss peak was observed in the loss spectra within our frequency and temperature limits. The variation of ε" curves with the applied frequency is similar to the frequency dependence of ε'. This correlation of ε' and ε" with frequency is associated with capacitance values experimentally. ε" decreases gradually with increasing frequency due to dielectric relaxation. It can be said that the contribution to relaxation is due to interfacial polarization and DC conductivity based on the shape of the plot.

3.4 Electric Modulus

Another useful way to interpret the relaxation phenomenon apart from the permittivity and AC conductivity formalism is the electric module formalism. Electric modulus formalism is a method that has been used and accepted in recent years (Hernandez *et al.*, 2010). A different perspective such as electric modulus will give us more specific results. Since electrode polarization, absorption and interactions of impurities can be neglected in the electric modulus formalism, large variations in components of complex dielectric permittivity can be minimized. The electrical modulus is described as inverse of the complex dielectric permittivity via (Psarras *et al.*, 2011):

$$M^* = \frac{1}{\varepsilon^*} = \frac{1}{\varepsilon' - j\varepsilon''} = M' + jM'' \quad (6)$$

where M' and M" are the real and imaginary components of the electric modulus, respectively. M' and M" can be found with the following formulas (Ray *et al.*, 2007):

$$M' = \frac{\varepsilon'}{[(\varepsilon')^2 + (\varepsilon'')^2]}, \; M'' = \frac{\varepsilon''}{[(\varepsilon')^2 + (\varepsilon'')^2]} \quad (7)$$

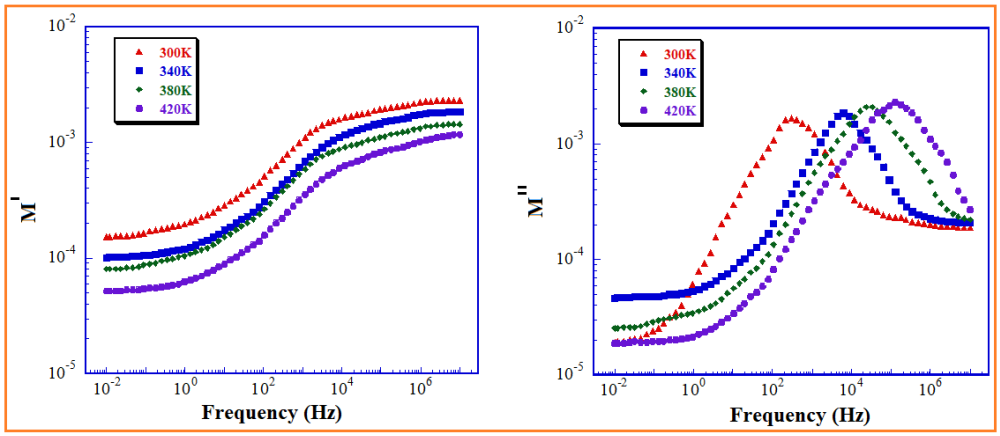

Fig. 7. (a) real part and (b) imaginary part of electric modulus.

Figure. 7 represents the variation of the real and imaginary parts of electric modulus with frequency at different temperatures. As can be seen from Figure.7 (a), the real part of the modulus takes small values in the low-frequency region. This confirms that the contribution of electrode polarization and electrode effects is small in this regime (Howell *et al.*, 1974). In all temperature measurements, the M' reached a constant maximum due to the relaxation process towards high frequencies. Frequency-dependent M" behavior at various temperatures was shown in Figure. 7 (b). The peak maximums shifted towards higher frequencies as the temperature increased. It can be concluded that the frequency regime below peak maximum defines the range of mobile charge carriers. It can also be said that in the regime above the maximum, the charge carriers are limited to potential wells that are mobile at short distances.

4. Conclusions

Herein, the composite films were prepared by the hot press method to investigate impedance characteristics, AC conductivity, and dielectric behaviors of SWCNT/VE binary composites depending on frequency and temperature. The impedance analyzer was used over a frequency range of 10^{-2} Hz – 10^{7} Hz to investigate the effect of temperature on the electrical impedance characteristics. Bode and Nyquist graphs were plotted and the results were interpreted with the Cole-Cole approach. When Nyquist graphs are examined, it is seen that the semi-circle with the smallest diameter belongs to the measurement made at 420 K. Since the diameter and conductivity are inversely proportional, it can be concluded that the increase in temperature enhances the AC conductivity. The conductivities at all temperatures exhibit power-law behavior. The SWCNT loaded matrix has constant conductivity since current flows preferably through the conductive nanotube phase at low frequencies. The conductivity became frequency-dependent after 100 Hz frequency and showed a linear behavior with increasing frequency value. Considering the effect of temperature on the AC electrical conductivity performance of the

material; it can be said that the high-temperature performance is better than that of low temperature. The highest AC conductivity of the order of 5.10^{-2} S/cm was achieved for SWCNT of 1 wt. % to the vinyl ester matrix at 420 K. Analysis of dielectric permittivity functions reported that Maxwell-Wagner-Sillars processes are the dominant mechanism affecting the dielectric constant at low-frequency regions. It has been found that at high frequencies, the polarization mechanisms lose their effectiveness, and the dielectric constant decreases. It also has been revealed that the dielectric properties of the SWCNT/VE/GFRP are affected by temperature variation. It was observed that the dielectric loss in the material increased with increasing temperature. Benefiting from the electric modulus formalism apart from permittivity formalism, dielectric relaxation was analyzed. It is revealed from the frequency dependence of the electrical modulus spectra that the dielectric relaxation detected at low frequencies at room temperature (300K) was related to the MWS process at the SWCNT-polymer interfaces. The relaxation peaks for increasing temperatures (340K-420K) shifted to higher frequencies due to the reorientation of the dipolar groups. The results obtained from the single-walled carbon nanotube-doped vinyl ester-based polymer composite developed for this study are expected to technically improve the design of the sensor and electromagnetic shielding applications.

ACKNOWLEDGEMENTS

The author thanks to Literatür Kimya for manufacturing composites.

References

Almond, D.P., West, A.R., Grant, R.J. (1982) Temperature dependence of the ac conductivity of Naβ-alumina. Solid State Communications, 44(**8**):1277–1280.

Almuhammadi, K., Bera, T.K., Lubineau, G. (2017) Electrical impedance spectroscopy for measuring the impedance response of carbon-fiber-reinforced polymer composite laminates. Composite Structures, 168:510-521.

An, Q., Rider, A. N., Thostenson, E. T. (2013) Hierarchical composite structures prepared by electrophoretic deposition of carbon nanotubes onto glass fibers. ACS Applied Materials and Interfaces, 5(**6**):2022–2032.

Anju, V.P and Narayanankutty, S.K. (2019) High dielectric constant polymer nanocomposite for embedded capacitor applications. Materials Science & Engineering B, 249:114418.

Antonucci, V., Faiella, G., Giordano, M., Nicolais, L., Pepe, G. (2007) Electrical properties of single walled carbon nanotube reinforced polystyrene composites. Macromolecular Symposium, 247(**1**):172–181.

Avilés, F., May-pat, A., López-manchado, M. A., Verdejo, R., Bachmatiuk, A., (2018) A comparative study on the mechanical, electrical and piezoresistive properties of polymer composites using carbon nanostructures of different topology. European Polymer Journal, 99:394–402.

Boukheir, S., Samir, Z., Belhimria, R., Kreit, L., Achour, M.E., Eber, N., Costa, L.C., Oueriagli, A, Outzourhit, A. (2018) Electric modulus spectroscopic studies of the dielectric properties of carbon nanotubes/epoxy polymer composite materials. Journal of Macromolecular Science, Part B: Physics, 57(**3**) 210-221.

Belhimria, R., Samir, Z., Boukheir, S., Teixeira, S.S., Achour, M.E., Casaos, A.A., Dominguez, J.M.G., Costa, L.C., Hasnaoui, M.E. (2021) Thermal and dielectric properties of carbon nanotubes/graphite/polyester ternary composites. Journal of Composite Materials, 55 (**25**) 3741–3750.

Bouzerara, R., Achour, S., Tabet, R. & Zerkout, N. S. (2011) Synthesis and characterization of ZnO/PVA composite nanofibres by electrospinning. International Journal of Nanoparticles, 4(**1**):10–19.

Daliri, O.S., Faller, L.M., Farahani, M., Roshanghias, A., Oberlercher, H., Mitterer, T., Araee, A., and Zangl, H. (2018) MWCNT-Epoxy nanocomposite sensors for structural health monitoring. Electronics, 7:143.

Dang, Z.M., Shehzad, K., Zha, J.W., Hussain, T., Jun, N., Bai, J. (2011) On refining the relationship between aspect ratio and percolation threshold of practical carbon nanotubes/polymer nanocomposites. Japanese Journal of Applied Physics, 50(**8**):080214.

Dang, Z.M., Yao, S.H., Xu, H.P. (2007) Effect of tensile strain on morphology and dielectric property in nanotube/polymer nanocomposites. Applied Physics Letters, 90(**1**):012907.

Das, A and Dobbidi, P. (2021) Impedance spectroscopy and ac conductivity in $Ba_{0.5}Sr_{0.5}TiO_3$−$Ca_{10}(PO_4)_6(OH)_2$ ceramic composites: An electrical approach to unveil biocomposites. ACS Biomaterials Science and Engineering, 7:2296-2308.

Ganesh, G. K. B. N. V. S., Yadav, A., Hiremath, M. M., Prusty, R. K., Ray, B. C. (2020) Enhancement of mechanical properties of glass fiber reinforced vinyl ester composites by embedding multi-walled carbon nanotubes through solution processing technique. Materials Today Proceedings, 27(**2**):1045-1050.

Helseth, L. (2018) Electrical impedance spectroscopy of multiwall carbon nanotube–PDMS composites under compression. Material Research Express, 5:105002.

Hernandez, M., Carretero-Gonzalez, J., Verdejo, R., Ezquerra, T.A., Lopez-Manchado, M.A. (2010) Molecular dynamics of natural rubber/layered silicate nanocomposites as studied by dielectric relaxation spectroscopy and dynamic mechanical spectroscopy. Macromolecules, 43:643–651.

Ho, C.H., Liu, C.D., Hsieh, C.H., Hsieh, K.H., and Lee, S.N. (2008) High dielectric constant polyaniline/poly (acrylic acid) composites prepared by in situ polymerization. Synthetic Metals, 158:630-637.

Howell, F.S., Bose, R.A., Macedo, P.B., Moynihan, C.T. (1974) Electrical relaxation in a glass-forming molten salt**.** Journal of Physical Chemistry, 78(**6**):639-648.

Jonscher, A.K. (1977) The 'universal' dielectric response. Nature, 267:673–679.

Jyoti, J., Kumar, A., Dhakate, S.R., Singh, B.P. (2018) Dielectric and impedance properties of three dimension graphene oxide-carbon nanotube acrylonitrile butadiene styrene hybrid composites, Polymer Testing, 68:456–466.

Kuilla, T., Bhadra, S., Yao, D., Kim, N.H., Bose, S., Lee, J.H. (2010) Recent advances in graphene based polymer composites. Progress in Polymer Science, 35(**11**):1350–1375.

Liang, Y., Liang, X., Zhang, Z., Li, W., Huo, X., Peng, L. (2015) High mobility flexible graphene field-effect transistors and ambipolar radio-frequency circuits. Nanoscale, 7:10954–10962.

Lvovich, V.F. (2012) Impedance Spectroscopy Applications to Electrochemical and Dielectric Phenomena. Wiley, New Jersey.

Mahapatra, S.P., Sridhar, V. & Tripathy, D. K. (2008) Impedance analysis and electromagnetic interference shielding effectiveness of conductive carbon black reinforced microcellular EPDM rubber vulcanizates. Polymer Composites, 29:465–472.

Mergen, O. B., Umut, E., Arda, E., Kara, S. (2020) A comparative study on the AC/DC conductivity, dielectric and optical properties of polystyrene/graphene nanoplatelets (PS/GNP) and multi-walled carbon nanotube (PS/MWCNT) nanocomposites. Polymer Testing, 90:106682.

Philipose, U.; Jiang, Y.; Western, B.; Harcrow, M.; Littler, C.; Sood, A.; Zeller, J.W.; Lineberry, B.; Syllaios, A.J. (2021) Impedance Analysis and Noise Measurements on Multi Walled Carbon Nanotube Networks. Materials, 14:7509.

Psarras, G.C., Siengchin, S., Karahaliou, P.K., Georga, S.N., Krontiras C.A., Karger-Kocsis, J. (2011) Dielectric relaxation phenomena and dynamics in polyoxymethylene/polyurethane/alumina hybrid nanocomposites. Polymer International, 60:1715–1721.

Puertolas, J.A., García-García, J.F., Pascual, F.J., Gonzalez-Domínguez, J.M., Martínez, M.T., Anson-Casaos, A. (2017) Dielectric behavior and electrical conductivity of PVDF filled with functionalized single-walled carbon nanotubes. Composites Science and Technology, 152:263–274.

Ray, D. K., Himanshu, A .K., Sinha, T.P. (2007) Structural and low frequency dielectric studies of conducting polymer nanocomposites. Indian Journal of Pure Applied Physics, 45:692-699**.**

Samir, Z., Merabet, Y. E., Graca, M.P.F, Teixeira, S. S., Achour, M.E., Costa, L.C. (2017) Dielectric behaviour of carbon nanotubes particles-filled polyester polymer composites. Journal of Composite Materials, 51(**13**):1831–1837.

Savi, P., Giorcelli, M., and Quaranta, S. (2019) Multi-Walled Carbon Nanotubes Composites for Microwave Absorbing Applications. Applied Sciences, 9:851.

Seng, L.Y., Wee, F.H., Rahim, H.A., Malek, F., You, K.Y., Liyana, Z., Jamlos, M.A., Ezanuddin A.A.M. (2018) EMI shielding based on MWCNTs/polyester composites. Applied Physics A, 124-140.

Tsonos, C. (2019) Comments on frequency dependent ac conductivity in polymeric materials at low frequency regime. Current Applied Physics, 19(**4**):491–497.

Zhu, J., Yang, D., Yin, Z., Yan, Q., Zhang, H. (2014) Graphene and graphene-based materials for energy storage applications. Small, 10(**17**):3480–3498.

Submitted: 17/01/2022
Revised: 06/04/2022
Accepted: 17/04/2022
DOI : 10.48129/kjs.19891